# A new set point in the selection of the αβTCR T cell repertoire imposed by the pre-TCR

Elena R. Bovolenta[1], Eva M. García-Cuesta[2], Lydia Horndler[1] Julia Ponomarenko[3,4], Wolfgang W. Schamel[5,6], Mario Mellado[2], Mario Castro[7], David Abia[8], Hisse M. van Santen[1]*[id]

[1]Immune System Development and Function Unit, Centro Biología Molecular Severo Ochoa, Consejo Superior de Investigaciones Científicas/Universidad Autónoma de Madrid (CSIC/UAM), 28049 Madrid, Spain; [2]Department of Immunology and Oncology, Centro Nacional de Biotecnología, Consejo Superior de Investigaciones Científicas (CSIC), 28049 Madrid, Spain; [3]Centre for Genomic Regulation (CRG), The Barcelona Institute of Science and Technology, 08003 Barcelona, Spain; [4]Universitat Pompeu Fabra (UPF), 08002 Barcelona, Spain; [5]Signalling Research Centers BIOSS and CIBSS and Department of Immunology, Faculty of Biology, University of Freiburg, Freiburg, Germany; [6]Centre for Chronic Immunodeficiency (CCI), University Clinics and University of Freiburg, Freiburg, Germany; [7]Grupo Interdisciplinar de Sistemas Complejos, Escuela Técnica Superior de Ingeniería, Universidad Pontificia Comillas de Madrid, 28015 Madrid, Spain; [8]Servicio de Bioinformática, Centro Biología Molecular Severo Ochoa, CSIC/UAM, 28049 Madrid, Spain.

*Address correspondence to Hisse M. van Santen, Centro de Biología Molecular Severo Ochoa, calle Nicolás Cabrera 1, Cantoblanco, Madrid 28049, Spain. Phone: 34-911964682; FAX: 34-911964420; e-mail: hvansanten@cbm.csic.es; id: ORCID 0000-0003-0769-4511.

**Abstract**

Signaling via the T Cell Receptor (TCR) is critical during the development, maintenance and activation of T cells. Quantitative aspects of TCR signaling have an important role during positive and negative selection, lineage choice and ability to respond to small amounts of antigen. By using a mutant mouse line expressing a hypomorphic allele of the CD3ζ chain, we show here that the strength of pre-TCR-mediated signaling during T-cell development determines the diversity of the TCRβ repertoire available for positive and negative selection, and hence of the final TCR$\alpha\beta$ repertoire. This finding uncovers an unexpected, pre-TCR signaling-dependent and repertoire-shaping role for $\beta$-selection beyond selection of in-frame rearranged TCRβ chains. Our data furthermore support a model of pre-TCR signaling in which the arrangement of this receptor in stable nanoclusters determines its quantitative signaling capacity.

**Introduction**

Signaling via the T Cell Receptor (TCR) is induced upon its interaction with cognate peptide-Major Histocompatibility Complex (pMHC) ligands. The TCR has low affinity for pMHC (1–3), but is able to cause the activation and response of the mature T cell upon exquisitely specific recognition of a small number of these pMHC ligands on professional antigen presenting cells or target cells (4–6). The molecular mechanisms that resolve the apparent contradiction between low affinity, specificity and high sensitivity are of interest because of the crucial role of TCR-mediated signaling in guaranteeing protective immunity and homeostasis. Their understanding can identify targets that can be used to control the immune response in therapeutic settings. In previous work, we and others identified one of these mechanisms, showing that the TCR organizes itself in nanoclusters at the T cell surface, already before antigenic stimulation, and presenting evidence that these TCR nanoclusters provide the T cell with enhanced sensitivity for its pMHC ligands (7–9). Furthermore, we could show that, concomitant with their differentiation from a naïve into a memory state, T cells increase sensitivity for their cognate ligand by enrichment for TCR nanoclusters (8–10). However, we have very little insight into the relevance of this mechanism during the stepwise developmental process that results in the generation of MHC-restricted self-tolerant mature T cells. Such knowledge is important, given that modulation of TCR signaling strength at particular T cell developmental stages determines the make-up and functional capacity of the mature T cell repertoire (11–13).

We previously demonstrated that the mutation of a single amino acid in the transmembrane domain of the TCR-associated CD3ζ chain impairs the formation of TCR nanoclusters and affects the TCR sensitivity of mature T cells (8). Based on this finding, we have generated a new mutant mouse model to address the role of TCR nanoclusters formation and T cell sensitivity in an organismal setting. We present an analysis of the successive T cell developmental stages in such mice, and show that the mutation impairs the maturation of T cell progenitors with in-frame re-arranged TCRβ genes, at one of the earliest T cell developmental checkpoints, which is dependent on signaling through the pre-TCR. The mutation converts CD3ζ into a hypomorphic mutant that reduces intrinsic and downstream signaling capacity of the pre-TCR, suggesting an important role for pre-TCR nanoclustering in its function. Using a next generation sequencing approach, we furthermore provide direct evidence for a new and important role of pre-TCR signaling intensity in shaping the diversity of the TCRβ repertoire.

**Results**

*L19A mice have a defect in early thymic αβT cell differentiation*

We previously showed that a Leucine to Alanine mutation at position 19 (L19A) of the murine CD3ζ transmembrane domain reduced TCR nanoclustering, concomitant with a decrease in T cell sensitivity (8). We generated transgenic mice expressing wild type or L19A CD3ζ-GFP fusion proteins under control of the hCD2 promoter and enhancer-regulated transgene cassette (14) and backcrossed these mice to a *Cd3z*$^{-/-}$ background (15) so that the GFP-CD3ζ chains were the only CD3ζ chains expressed in these mice. Immunoblot analysis of whole lysates from total thymus and purified double-negative (DN) thymocytes showed the presence of ~100 kD covalently associated homodimers reactive with both CD3ζ- and GFP-specific antibodies (Suppl. Fig.. 1A and B). Homogeneous expression of the transgenic CD3ζ–GFP fusion proteins was detected by flow cytometry in all thymic subsets tested (Suppl. Fig. 1C). Mice on this background will be referred to as WT and L19A mice. We pooled the data of the two independent lines analyzed of each genotype, as we did not observe phenotypic differences between them (Suppl. Fig. 1D)

Thymi isolated from L19A mice contained 2- to 3-fold fewer cells than thymi from WT mice (Fig. 1A, upper graph). The DP, 4SP and 8SP populations were reduced in number whereas there was a relative increase in DN tymocytes, indicating a defect in thymocyte differentiation that was occurring at the DN stage in L19A mice (Fig. 1A, middle and lower graphs). Subdivision of the DN population into the DN1-DN4 subsets using the CD25 and CD44 markers (16)

revealed similar percentages and numbers of $CD44^+CD25^-$ DN1 and $CD44^+CD25^+$ DN2 cells in L19A and WT thymi, but a relative accumulation of $CD44^-CD25^+$ DN3 cells and a relative and absolute reduction of $CD44^-CD25^-$ DN4 cells in L19A thymi as compared to WT thymi (Fig. 1B). Thus, the earliest observable defect in αβ-T cell differentiation in L19A mice occurred at the transition from the DN3 to DN4 stage. The absolute numbers of DN4 thymocytes and the percentages of DN3 and DN4 mutant thymocytes were significantly different from those of CD3ζ–deficient mice (Fig. 1B), which present an almost complete loss of the DN4 population, indicating that the L19A CD3ζ chain could at least partially overcome defects imposed by *Cd3z* deficiency on pre-TCR function.

The DN3 to DN4 transition depends on the formation and function of the pre-TCR, a CD3-associated heterodimer of an in-frame rearranged TCRβ chain and an invariant pTα chain (17). DN3 thymocytes that have rearranged the TCRβ chain (DN3b thymocytes) can be distinguished from their immediate precursors (DN3a thymocytes) by phenotypical changes induced upon pre-TCR signaling, including an increase in cell size (18). Applying this criterion, we quantified the percentage of DN3a and DN3b thymocytes in the DN population of L19A and WT mice using as a reference DN3 thymocytes from *Cd3e*-deficient mice, which can rearrange their *Tcrb*-locus, but cannot express the pre-TCR and do not reach the DN3b stage (19). L19A thymi contained significantly more DN3a and fewer DN3b thymocytes than WT thymi. (Fig. 1C). This lag in T cell development was not due to the inability of L19A thymocytes to rearrange their *Tcrb*-locus, as intracellular staining for TCRβ in the DN3b and DN4 populations of WT and L19A thymi showed an equal intensity (Fig. 1D). Moreover, cell surface expression of the pre-TCR on the DN3b-enriched $CD44^-CD25^{lo}$ population and $CD44^-CD25^-$ DN4 cells, measured by extracellular staining with an antibody against the TCRβ chain, was indistinguishable between L19A and WT mice (Fig. 1E). Likewise, cell surface expression of CD3ε and pTα and expression of the transgenic CD3ζ-GFP chain was equal for WT and L19 DN3b and DN4 thymocytes (Suppl. Fig. 2A-D). We found that cell surface expression and stoichiometry of the cell surface-displayed complexes of the pre-TCR was not affected by the L19A mutation in cell lines derived from the pre-T cell line SCB.29 (20), rendered *Cd3z*-deficient via CRISPR-Cas9-mediated gene edition and reconstituted with WT or L19A CD3ζ-GFP (Suppl. Fig. 3A-C). Immunoprecipitation experiments of the pre-TCR in these cell lines showed that the ratio of CD3ζ over CD3ε in immunoprecipitates with TCRβ- and CD3ε-specific antibodies was lower in the L19A cell lines than in WT cell lines, suggesting that under these conditions the association between CD3ζ and the other components of the pre-TCR was weaker (Suppl. Fig. 3D).

*The L19A mutation impairs pre-TCR signaling and function.*

Signaling via the pre-TCR promotes the survival and proliferation of DN3 thymocytes with an in-frame rearranged *Tcrb* locus and permits their differentiation to the DP stage in a process termed β-selection (21). In order to capture the physiological signaling status of pre-TCR in WT and L19A thymocytes, we determined the activation level of pre-TCR signaling pathway components directly *ex vivo*, without stimulation with anti-CD3 or -TCRβ antibodies. We first focused on the proline-rich sequence (PRS) of the intracellular domain of CD3ε, which is known to be selectively exposed in active TCRs and can be detected by intracellular staining with the APA1/1 mAb (22, 23). We used DN thymocytes from KI-PRS mice as a negative control for staining, as the key Proline residues in the CD3ε PRS of these mice are mutated to Alanine, abrogating recognition by the APA1/1 mAb (24). Freshly isolated DN3b and DN4 thymocytes from WT and L19A mice, identified as $CD44^{-}CD25^{lo}$ and $CD44^{-}CD25^{-}$ DN thymocytes respectively, showed specific staining (Fig. 2A). However, L19A DN3b and DN4 thymocytes showed a significantly lower APA1/1 staining intensity than WT DN3b and DN4 thymocytes, consistent with reduced pre-TCR signaling. This was not due to a lower expression level of CD3ε in L19A thymocytes (see Suppl. Fig. 2C), but indicated fewer active pre-TCRs in L19A thymocytes. The high and equal level of APA1/1 staining observed in WT and L19A DN3a thymocytes was expected, as in absence of TCRβ the CD3ε chains are retained in the ER and are in the conformation recognized by APA1/1 mAb (25). We also measured phosphorylation of the receptor-proximal signaling molecule ZAP70 in freshly isolated thymocytes, including treatment with the Lck inhibitor A770041 as a specificity control. L19A DN3b and DN4 thymocytes showed decreased phosphorylation of Y319 of ZAP70 as compared to WT thymocytes (Fig. 2B). No such differences were found in DN3a thymocytes. We extended these data using the WT and L19A pre-T cell lines. Steady state CD3ε ITAM phosphorylation was decreased in the L19A cell lines as compared to the WT cell lines (Suppl. Fig. 4A). Upon stimulation of these cell lines with a CD3ε-specific antibody we observed decreased CD3ζ and ZAP70 phosphorylation in L19A cell lines as compared to WT cell lines (Suppl. Fig. 4B and C). We measured the functional consequences of this impaired signaling, focusing on induction of markers associated with differentiation, proliferation and survival. Upregulation of the transferrin receptor (CD71; Fig. 2C) and the large neutral amino acid transporter subunit CD98 (Fig. 2D) was significantly impaired in DN3b and particularly in DN4 thymocytes of L19A mice. CD25 cell surface expression, downregulation of which is reduced in mice with defects in pre-TCR components and associated signaling molecules (26, 27) and is considered a marker for pre-TCR signal intensity received by DN cells, was higher in L19A DN3 thymocytes than in WT DN3 thymocytes (Fig. 2E). BrdU-positive, proliferating DN3 and DN4 L19A thymocytes were

clearly diminished in numbers as compared to the corresponding WT thymocytes (Fig. 2F) and L19A thymocytes were also more prone to undergo apoptosis than WT thymocytes (Fig. 2G). These results clearly indicated that the function of the pre-TCR in L19A mice was impaired, providing an explanation for the observed differentiation defect.

*CD3ζ regulates the motion and cell surface organization of the pre-TCR*

Most available data support the concept that the pre-TCR signals in the absence of ligands and pre-TCR dimers have been proposed as the unit of signaling (28). Given our previous findings on the effect of the L19A mutation on TCR organization, we assessed the distribution of the pre-TCR at the cell surface of WT and L19A thymocytes. We purified DN3 and DN4 thymocytes excluding the 1% GFP-brightest cells that were not amenable to individual particle observation, adhered them to fibronectin-coated cover slips and analyzed them via TIRF microscopy (Fig. 3A). We used the CD3ζ-coupled GFP as the label to track the pre-TCR complexes, as cell surface labeling of WT and L19A DN thymocytes showed a strong correlation between GFP signal and CD3ε staining (Suppl. Fig. 2E). Only fluorescent particles that were continuously detectable and did not fuse or split during a time period of at least 5 seconds were analyzed. The average number of particles detected at the cell surface of L19A DN thymocytes was significantly lower than observed for WT DN thymocytes (Fig. 3B), even though no difference in the total level of expression of pre-TCR was observed for these populations (Fig. 1E and Suppl. Fig. 2A-D). L19A pre-TCR particles had an increased diffusion rate as compared to WT particles (Fig. 3C). There was no significant difference in distribution between confined, free and directed diffusion of mobile particles (Fig. 3D) excluding a shift in diffusion mode as the mechanism underlying the overall speed-up. Particles displayed a wide range of fluorescence intensities, suggesting that pre-TCRs grouped in clusters of various sizes (Fig. 3E). However, L19A particles displayed a lower average intensity than WT particles, with a marked underrepresentation of higher intensity particles. These data are compatible with the notion that WT pre-TCRs form stable nanoclusters and that the L19A mutation reduces their size.

*TCRβ repertoire diversity is regulated by the intensity of pre-TCR signaling.*

In order to determine whether the intensity of pre-TCR signaling has a functional impact on the β-selected TCRβ repertoire, we assessed TCRβ diversity in post-β-selection, large $CD69^-$ DP WT and L19A thymocytes, which have not yet been subject to negative and positive selection (Fig. 4A). We determined V, D, J and CDR3 identity of each TCRβ chain by amplifying their cDNAs via an unbiased 5' RACE protocol and high-throughput amplicon sequencing. Both the number of recovered cells and in-frame reads obtained from them were higher for WT than

L19A thymi (Table 1). This was in line with the finding that WT cells produced more early DP thymocytes. (Suppl. Fig. 5A). We determined the effective number of clones in each repertoire by calculating Hill numbers $^{q}D$ via rarefaction and extrapolation methods (29), being $^{0}D$ the effective number of different clones. Rarefaction curves for the WT DP repertoires separated almost completely from the curves for L19A DP repertoires (Fig. 4B) and the observed and estimated numbers of clones were significantly higher in WT than L19A DP repertoires (Table 1), indicating that TCRβ repertoires were more diverse in WT mice than in L19A mice. Calculating diversity using q values of 1 and 2, thereby providing more weight to the more abundant clones within the populations, gave an essentially identical pattern of diversities (Suppl. Fig. 5B and C). The latter provided evidence for the robustness of the analysis of early DP repertoire diversity. The coverage (29) for each mouse was above 0.98 so the extrapolated parts of the curve were close to the asymptotic diversity and guaranteed that the estimation of the diversity of the repertoires was accurate (Suppl. Fig. 5D). Furthermore, we addressed the effect of sample size on diversity estimates and found that this was not a confounding factor in the approaches we used (Suppl. Text 1). We also compared diversity of the TCRβ repertoire in WT and L19A $CD25^{hi}CD44^{-}$ DN3 thymocytes that contain cells that have rearranged the *Tcrb* gene segments but should have undergone little or no pre-TCR-mediated selection and expansion (Fig. 4A). There were no significant differences in the number of recovered cells or in the number of in-frame reads (Table 1). No clear separation of rarefaction curves derived from the WT and L19A DN3 repertoires was observed (Fig. 4C) and the observed and estimated numbers of clones in WT and L19A DN repertoires were not significantly different (table 1). Collectively, these findings underscored that the difference in repertoire diversity at the early DP stage was a consequence of reduced signaling by the pre-TCR during β-selection.

## Discussion

The role of pre-TCR signaling intensity in the transition from the DN3 to the DN4 and early DP stages and its consequences for the repertoire of thymocytes that can undergo positive and negative selection have barely been addressed. We demonstrate in primary murine DN thymocytes and pre-T cell lines that the L19A mutation reduces steady state and antibody-induced activation levels of signaling components within and downstream of the pre-TCR. We provide direct evidence that the reduced intensity of pre-TCR signaling in L19A mice has a quantitative impact on the TCRβ diversity of the population of early DP thymocytes that still need to undergo positive and negative selection. This latter finding implies that during β-

selection not all DN precursors with in-frame rearranged *Tcrb* genes mature but that pre-TCR signaling efficiency imposes a filter on the emerging repertoire. Our data are compatible with a mechanism in which pre-TCR signaling intensity is regulated by nanoclusters of the pre-TCR.

We explain our findings via a model in which pre-TCR signaling intensity determines the likelihood that a DN thymocyte reaches the early DP stage. Continuous signaling would be necessary to maintain both proliferation and survival programs active during this transition, with lower intensities of signaling increasing the likelihood that a clone will die out. Within the context of the L19A mutation, we favor the interpretation that the L19A mutation interferes with the organization of the pre-TCR, reducing the number and size of nanoclusters displayed at the cell surface and thereby the signaling capacity of the pre-TCR, with a potentially weaker association of the L19A CD3ζ chain with the rest of the pre-TCR complex representing an alternative mechanism per se or an integral part of the mechanism underlying the reduction in nanocluster formation. Our previous work on the TCR has shown that nanoclusters provide increased antigen-sensitivity to T cells (7), likely via cooperative signaling mechanisms within such clusters (30), and that the degree of organization of TCRs into nanoclusters scales with antigen sensitivity of the T cell (8). In the absence of at least canonical interactions with pMHC ligands (31), regulation of pre-TCR signaling would be expected to rely on pre-TCR intrinsic mechanisms. The most membrane-proximal pre-TCR signaling event that we found impaired in L19A DN3b and DN4 thymocytes is the conformational change that exposes the intracellular PRS of CD3ε (32). The conformational change is critical for pre-TCR-dependent signaling as β-selection is severely impaired in mice with mutations in the extracellular stalk domain of CD3ε that abrogate this conformational change (23, 33) and in mice with a mutated or deleted PRS (24, 34). This event correlates in mature T cells with dislodging of the CD3ε intracellular domain from the inner membrane leaflet, facilitating its recognition by the TCR-associated signaling machinery (35, 36) and is induced and maintained by ligand binding (37). The recent finding of direct binding of Lck to CD3ε that depends on the conformational change (38) provides a mechanism in which a key initiator of pre-TCR signaling is recruited in a graded fashion to this complex in function of the degree of conformational change. Our data support the notion that the fraction of pre-TCRs undergoing a conformational change depends on the degree of their organization in nanoclusters. The known role of the CD3ζ transmembrane in TCR nanoclustering (8) and the here reported correlation between signaling capacity and mobility and fluorescence intensity of pre-TCR particles in WT and L19 thymocytes make this a likely mechanism. Assuming that the pre-TCR oscillates between a signaling-competent, CD3ε-exposing stage and a non-competent stage, as has been proposed for the TCR (39, 40), we

speculate that this exposure is stabilized by its interaction with neighboring pre-TCR complexes within pre-TCR nanoclusters. This interaction could in part rely on the inherent ability of the pTα extracellular domain to form homodimers, but would need the transmembrane domain of CD3ζ. The range of fluorescent intensities that we observe in the WT thymocytes and their stability over time support the existence of nanoclusters bigger than the so far proposed pre-TCR dimers (41, 42). The limits of resolution of TIRFM do not allow us to distinguish between the possibility that the observed particles represent pre-TCR nanoclusters of various sizes or whether these are stable membrane domains that contain more or less pre-TCRs. If pre-TCR signaling indeed depends on nanoclusters, this could provide new therapeutic targets for the treatment of T-ALL. TCR nanocluster integrity is regulated by specific membrane lipids (7, 9, 43, 44) and recent work on mature T cells in preclinical models of cancer immunotherapy have shown that manipulation of membrane cholesterol content in tumor-specific T cells can regulate their anti-tumor response (45). T-ALL depend on pre-TCR signaling for their maintenance (46–48) and interference with pre-TCR nanoclusters could therefore be a relevant therapeutic approach with druggable targets.

Our findings make clear that β-selection permits maturation of DN thymocytes with a range of pre-TCR-dependent signaling capabilities, and this likely has consequences for the final TCR repertoire if reduced signaling capacity is maintained during the TCR signaling-dependent differentiation steps. In the context of the L19A mutation it would be expected that the reduced signaling capacity is maintained in the DP thymocytes, as a recent report strongly suggests that nanoclustering of the TCR indeed occurs in these cells and is relevant for the outcome of positive and negative selection (44). Analysis of the 4SP to 8SP ratio in WT and L19A thymi also provides support for this notion, with L19A thymi having a lower ratio than WT thymi (data underlying Fig. 1A; 1.41 ± 0.67 vs 2.07 ± 1,13; $p<0.05$ unpaired two-tailed Student's T test). Lineage choice is determined by TCR signaling strength at the $CD8^{+}CD4^{low}$ stage of selection with a higher signaling capacity necessary for the CD4 lineage choice (49). It could be expected that TCRs with higher self-pMHC affinity would be allowed to mature, giving rise to a potentially auto-reactive T cell repertoire. In a general context, mutation or allelic variation of components involved in signaling via the pre-TCR and/or variation in their expression level, could be expected to have similar effects on pre-TCR signaling capacity of DN thymocytes, and promote the selection of higher affinity clones upon differentiation to the DP stage.

While the increased cell death observed in L19A DN thymocytes would be expected to decrease TCRβ diversity at the early DP stage, this loss might be compensated by the reduced proliferation capacity of these cells, causing the niche to be filled by fewer descendants of

each clone and thus allowing more room for additional clones. This is not the case, as both the number of clones in the large $CD69^-$ DP compartment is smaller in L19A mice (Fig. 4B and table 1) and the numerical size of this compartment is significantly smaller in the L19A mice as compared to WT mice (Suppl. Fig. 5D). In a stochastic model for the relationship between diversity loss, proliferation and death rate (Suppl. Text 2) we find that the loss of diversity scales with the ratio of rate of cell death over proliferation rate ('extinction probability'). Using as an approximation of changes in these rates the relative differences in percentages of proliferation and cell death (Fig. 2F and G) the extinction probability of L19A thymocytes in transition from DN to early DPs would be 3-4 fold higher than for WT thymocytes. Thus reduced proliferation and increased propensity to die do not compensate opposing effects on repertoire diversity but contribute both to the reduction in diversity we observe.

The signaling capacity-dependent selection step we describe here does not appear to select particular molecular features of the TCRβ chain. We did not find changes in CDR3 length between DN3 and early DP thymocytes, or between WT and L19A DN3 and early DP thymocytes (Suppl. Fig. 5E), and an in-depth analysis of representation of VDJ combinations and the CDR3 amino acid sequences did not show clear patterns that were favored in either WT or L19A early DP thymocytes (Suppl. Fig. 5F and data not shown). These findings are compatible with the notion that the pre-TCR can signal independent of ligand engagement. They do not exclude the possibility that a non-canonical mode of pre-TCR – pMHC interaction takes place (31), taking into account that the reported variability in contacts between the TCRβ chain and the MHC class I molecule could preclude stringent selection of defined TCRβ features.

Our work shows that the intensity of pre-TCR signaling determines the diversity of the early TCRβ repertoire and proposes a mechanism for regulation of pre-TCR signaling strength by clustering. It also reveals that the pre-TCR imposes an unpredicted set point in the selection of the mature αβTCR T cell repertoire.

## Materials and Methods

### *Mice*

CD3ζWT-GFP and CD3ζL19A-GFP transgenic mouse lines were generated in the CNB/CBMSO transgenesis facility. The previously described CD3ζWT-GFP and CD3ζL19A-GFP cDNA sequences (8) were amplified with 5' and 3' flanking oligos containing an *Eco*RI and *Sal*I site, respectively, and cloned into the *Eco*RI and *Sal*I sites of the transgenic cassette vector p29Δ2 in which expression of the inserted DNA fragment is regulated by the hCD2 promoter and enhancer (14). Transgenic mice were obtained by injecting the promoter, transgene and enhancer sequences-containing *Not*I fragment into C57BL/6JxSJL F1 1-cell stage embryos and transplanting the embryos in pseudo-pregnant foster mothers. Two male founder mice for each transgenic construct (WT-F10, WT-F19, L19A-F13 and L19A-F23), initially identified via southern blot using a GFP-specific probe, were selected and backcrossed once with C57BL/6J females to check for germ line transmission and further backcrossed to a *Cd3z*$^{tm1Lov}$ knock-out background (15). Relative copy numbers of the transgenes, as determined by quantitative PCR analysis of genomic DNA, were 3-5 fold higher for the L19A lines as compared to the WT lines, which displayed similar copy numbers (Suppl. Fig. 1E). Mice backcrossed for 2 to 5 generations to the C57BL/6J background, homozygous for the *Cd3z*$^{tm1Lov}$ allele and always carrying the transgene in hemizygosity were used for the experiments described in this manuscript. Knock-in mice with a PxxP to AxxA double mutation in the PRS of CD3ε were described previously (24). *Cd3e*$^{tm1Lov}$ knock-out mice were obtained from Jackson Laboratories (stock #004177) (19). Mice homozygous for the *Rag1*$^{tm1Mom}$ knock-out allele (50) were kindly provided by Dr. César Cobaleda (CBMSO, Madrid). Animals aged between 5 and 9 weeks were used for all experiments. Mice were maintained under SPF conditions in the animal facility of the CBMSO in accordance with applicable national and European guidelines. All animal procedures were approved by the ethics committees of the Consejo Superior de Investigaciones Científicas and the Comunidad Autónoma de Madrid (PRO-EX 68/14, PRO-EX 384/15 and PRO-EX 40.6/20).

### *Antibodies and reagents*

Antibodies used to detect the indicated mouse proteins were: CD4-PerCP, -A647, -FITC (RM4-5), CD8-biotin, -PerCP, -647 (53-6.7), CD11b-biotin (M1/70), purified CD16/32 (2.4G2), CD19-biotin (1D3), CD25-PerCP, -APC, -PE (3C7), Gr1-biotin (RB6-8C5), CD44-BV421, -PE and -APC (IM7); TCRβ-APC, -PE, and -BV421 (H57-597); CD3ε-PerCP, -APC, -PE and -biotin (2C11), NK1.1-biotin (PK136), purified pTα (2F5), CD3γε-APC (17A2), TCRγδ-biotin (GL3) and pZAP70(Y319)-

A674, obtained from BD Biosciences; F4/80-biotin (BM8), CD98-PE (RL388), CD8-BV421 (53-6.7), CD71-PE (R71217), all from eBioscience. Annexin V-PE, 7AAD and the APC-labeled anti-BrdU mAb (3D4) were purchased from BD Biosciences. The APA1/1 monoclonal antibody, which recognizes a conformational epitope of CD3ε, and its use as a probe for the conformational change of the TCR have been described previously (22). Where necessary, secondary antibodies (anti-rabbit A647 and anti-mouse A647 from ThermoFisher) or fluorescent probes (Streptavidin-PerCP and -APC from BD Biosciences, Streptavidin-PE from Invitrogen and Streptavidin-BV421 from Biolegend) were used.

*Flow cytometry*

Thymi were homogenized with 40 µm strainers and washed in phosphate-buffered saline (PBS) containing 1% bovine serum albumine (BSA). Single-cell suspensions were counted with a Scepter 2.0 Cell Counter and incubated with conjugated antibodies for 30 minutes at 4ºC after blocking Fc receptors using an anti-CD16/32 antibody. For intracellular staining the cytofix/cytoperm kit (BD #554714) was used according to provided instructions with incubation times for primary antibodies ranging from 30 min to overnight. For detection of apoptotic cells, a Annexin V kit (BD #560930) was used following the provided protocol. For detection of proliferation of primary thymocytes *in vivo* proliferation, mice were injected i.p. with 150µl of a BrdU solution (10 mg/ml). After 2 hours, mice were sacrificed and thymi were collected. Transmembrane proteins of thymocytes were labeled followed by fixation, permeabilization, DNAse treatment and anti-BrdU staining using a BrdU Flow Kit (BD #552598). Labeled cells were washed in PBS+1%BSA and acquired on a FACS Canto II (BD). Data was recorded in a low flow rate mode to ensure a good resolution of the labeling. Analyses were performed using FlowJo software (BD FlowJo LLC).

*TIRF Microscopy*

Pooled thymocyte suspensions from 2-3 WT or L19A mice were obtained and $Lin^-$ thymocytes were negative selected using Ly6c-, F4/80-, CD11b-, CD11c-, CD19-, B220-, NK1.1-, CD4 - and CD8-specific antibodies and subsequently sheep-anti-rat dynabeads (Invitrogen #11035). A second round of selection using a FACSAria Fusion cell sorter was performed on $Lin^-$ thymocytes to obtain DN $CD44^-$ thymocytes (DN3+DN4 populations) that express GFP levels under $10^3$ relative fluorescence units. This latter selection criterion, excluding the ~1% brightest DN cells, guaranteed that we could detect individual particles at the cell surface using

the TIRF setting. Sorted DN CD44$^-$ thymocytes were left to recover in RPMI containing 5% FBS for at least 2 hours. 30 minutes before TIRFM analysis, thymocytes were seeded on microscopy plates pretreated with fibronectin (10 μg/ml, 60 min, 37°C). Experiments were performed using a TIRF microscope (Leica AM TIRF inverted) equipped with an EM-CCD camera (Andor DU 885-CS0-#10-VP), a 100x oil-immersion objective (HCX PL APO 100x/1.46 NA) and a 488-nm diode laser. The microscope was equipped with incubator and temperature control units; experiments were performed at 37°C with 5% CO2. To minimize photobleaching effects before image acquisition, cells were located and focused using the bright field, and a fine focus adjustment in TIRF mode was made at 5% laser power, an intensity insufficient for single-particle detection that ensures negligible photobleaching. Image sequences of individual particles (500 frames) were acquired at 49% laser power with a frame rate of 10 Hz. The penetration depth of the evanescent field used was 90 nm. For the analysis, particles were detected and tracked using previously described algorithms (U-Track2; (51)) implemented in MATLAB. The intensity value for each particle was calculated by subtracting in each frame the background intensity from the particle intensity. In addition, to minimize photon fluctuations within a given frame, the particle intensity was represented as the average value (background subtracted) obtained over the first 20 frames. For the short-time lag diffusion coefficient ($D_{1\text{-}4}$), only tracks longer than 50 frames were used for further analysis; particles that merged or split were excluded. Individual trajectories were used to generate mean-square-displacement (MSD) plots that were required to extract the $D_{1\text{-}4}$ using the equation: $MSD = 4D1\_4t + \Delta 0$, where the Δ0 is the MSD offset at zero-time lag. Additional details can be found in (52).

*Analysis of TCRβ repertoire*

DN3a (CD4$^-$CD8$^-$CD25$^+$CD44$^-$) and blasting DP (CD4$^+$CD8$^+$CD69$^-$FCS$^{hi}$) thymocytes of WT and L19A 5-8 week-old male mice were purified by sorting. mRNA was extracted from purified thymocytes using the RNAeasy micro Kit (QIAGEN #74004). *Tcrb* amplicons were prepared using a 5'RACE-based protocol with the SMARTer Mouse TCR α/β Profiling Kit (Takara #634402) following the manufacturer's instructions. The *Tcrb* amplicons were purified using AmpureXP beads (Beckman Coulter #A63880) and sequenced in parallel via Illumina High Throughput Sequencing on an Illumina MiSeq (2x300nt) at the Centro Nacional de Análisis Genómico (CNAG-CRG) Barcelona, Spain). The quality of reads was assessed using FastQC (http://www.bioinformatics.babraham.ac.uk/projects/fastqc/). Raw sequencing reads were processed using the MiXCR v3.0.8 software (53) allowing identification of CDR3 sequences, determination of V, D and J genes and assembly of clonotypes by CDR3 sequences. Taking into

account the error rate of the sequencing methodology (54) a filter was applied to each library, grouping reads that differed in less than 3% of their CDR3 nucleotide sequence. Further analysis of clones was conducted using the iNEXT R package (29), in-house written R-scripts and VDJtools v1.2.2 (55). The ${}^{q}D$ was computed using a rarefaction/extrapolation algorithm and coverage was estimated using the same techniques.

*Statistical analysis*

Statistical parameters including the exact value of n, the means ± SEM are described in the text and Figure legends. All results were analyzed using GraphPad PRISM 7.0 (*p<0.05, ** p<0.01, *** p<0.001; **** p<0.0001 or the exact p value). TIRFM-Lag diffusion coefficient ($D_{1\text{-}4}$) and the mean fluorescent intensity of single particles were analyzed using a two-tailed Mann-Whitney nonparametric test. All other statistical analyses were performed using the parametric, two-tailed and unpaired t-test or the Mann-Whitney test.

*Data availability*

Raw sequencing data that underlie the analyses reported in Figure 4 and Supplementary Figure 5 have been uploaded to the Bioproject Sequence Read Archive and can be consulted at https://dataview.ncbi.nlm.nih.gov/object/PRJNA609042?reviewer=fompha0koeaebfaom3g640fqef

*Materials Availability Statement*

The mice generated in this study are available from the corresponding author with a completed Materials Transfer Agreement. Further information and requests for reagents may be directed to the corresponding author Dr. Hisse M. van Santen (hvansanten@cbm.csic.es)

*Supplementary Material*

Supplementary material consists of Supplementary texts 1 and 2, Supplementary Figures S1-S5 and Supplementary references.

**Acknowledgments**

We thank Cristina Prieto, Valentina Blanco, Tania Gomez and the CBMSO flow cytometry service for excellent technical assistance, Belen Pintado and Veronica Dominguez from the

CNB/CBMSO transgenic mouse facility for the generation of the CD3ζL19A-GFP and CD3ζWT-GFP mice, the CNAG-CRG for assistance with Amplicon-Seq and Andreas Krüger for providing us with the SCB29 cell line; Balbino Alarcon, Maria Luisa Toribio and our laboratory members for their expert advice and critical analysis of this manuscript. E.R.B. was supported by a FPI fellowship (BES-2014-068000, Subprograma Estatal de Formación del Programa Estatal de Promoción del Talento y su Empleabilidad, en el marco del Plan Estatal de Investigación Científica y Técnica y de Innovación 2013-2016) and an EMBO short term fellowship (#7272). This work was supported by Spanish Ministry of Economy and Competitiveness (MINECO) grants SAF2013-47975-R and SAF2016-76394-R and grant PID2019-104703GB-I00 from the Spanish Ministry of Science and Innovation (MICINN) to H.M.v.S. and FIS2016-78883-C2-2-P to M.C. W.W.S. was supported by the German Research Foundation (DFG) through BIOSS - EXC294 and CIBSS - EXC 2189, SFB854 (B19), FOR2799 (SCHA976/8-1) and SFB1381 (A9). The Centre for Genomic Regulation acknowledges support of the Spanish Ministry of Economy and Competitiveness, "Centro de Excelencia Severo Ochoa," the Centres de Recerca de Catalunya Program/Generalitat de Catalunya. The Centro de Biología Molecular Severo Ochoa has been supported by the Fundación Ramón Areces.

## Author Contributions

E.R.B. and H.M.v.S. conceived the project. E.R.B., L.H. and H.M.v.S. designed and conducted the experiments. E.M.G.C. conducted TIRF microscopy and performed analysis and interpretation of the obtained data. J.P., M.C. and D.A. analyzed and interpreted the TCRβ repertoire data, generating scripts necessary for visualization and interpretation of the results. W.W.S. and M.M. provided ideas, designed experiments and helped with interpretation of results. E.R.B. and H.M.v.S. analyzed and interpreted the data and wrote the manuscript. All other authors edited the manuscript.

## Declaration of interests

The authors declare that they have no conflict of interest.

## References

1. M. Corr, *et al.*, T cell receptor-MHC class I peptide interactions: affinity, kinetics, and specificity. *Science* **265**, 946–9 (1994).

2. K. Matsui, J. J. Boniface, P. Steffner, P. A. Reay, M. M. Davis, Kinetics of T-cell receptor binding to peptide/I-Ek complexes: correlation of the dissociation rate with T-cell responsiveness. *Proc Natl Acad Sci U S A.* **91**, 12862–6. (1994).

3. J. B. Huppa, *et al.*, TCR-peptide-MHC interactions in situ show accelerated kinetics and increased affinity. *Nature* **463**, 963–7 (2010).

4. S. Demotz, H. M. Grey, A. Sette, The minimal number of class II MHC-antigen complexes needed for T cell activation. *Science* **249**, 1028–30 (1990).

5. C. V. Harding, E. R. Unanue, Quantitation of antigen-presenting cell MHC class II/peptide complexes necessary for T-cell stimulation. *Nature.* **346**, 574–6. (1990).

6. D. J. Irvine, M. A. Purbhoo, M. Krogsgaard, M. M. Davis, Direct observation of ligand recognition by T cells. *Nature* **419**, 845–9. (2002).

7. W. W. Schamel, *et al.*, Coexistence of multivalent and monovalent TCRs explains high sensitivity and wide range of response. *J Exp Med* **202**, 493-503. Epub 2005 Aug 8. (2005).

8. R. Kumar, *et al.*, Increased sensitivity of antigen-experienced T cells through the enrichment of oligomeric T cell receptor complexes. *Immunity* **35**, 375–87 (2011).

9. A. Martin-Leal, *et al.*, CCR5 deficiency impairs CD4(+) T-cell memory responses and antigenic sensitivity through increased ceramide synthesis. *The EMBO journal*, e104749 (2020).

10. M. Castro, *et al.*, Receptor Pre-Clustering and T cell Responses: Insights into Molecular Mechanisms. *Frontiers in immunology* **5**, 132 (2014).

11. K. A. Hogquist, S. C. Jameson, The self-obsession of T cells: how TCR signaling thresholds affect fate “decisions” and effector function. *Nat Immunol* **15**, 815–23 (2014).

12. T. Nakayama, M. Yamashita, The TCR-mediated signaling pathways that control the direction of helper T cell differentiation. *Seminars in Immunology* **22**, 303–309 (2010).

13. M. Ciofani, J. C. Zúñiga-Pflücker, Determining γδ versus αβ T cell development. *Nat Rev Immunol* **10**, 657–663 (2010).

14. D. R. Greaves, F. D. Wilson, G. Lang, D. Kioussis, Human CD2 3’-flanking sequences confer high-level, T cell-specific, position-independent gene expression in transgenic mice. *Cell* **56**, 979–86 (1989).

15. P. E. Love, *et al.*, T cell development in mice that lack the zeta chain of the T cell antigen receptor complex. *Science* **261**, 918–21 (1993).

16. D. I. Godfrey, J. Kennedy, T. Suda, A. Zlotnik, A developmental pathway involving four phenotypically and functionally distinct subsets of CD3-CD4-CD8- triple-negative adult mouse thymocytes defined by CD44 and CD25 expression. *J Immunol* **150**, 4244–52 (1993).

17. M. Groettrup, *et al.*, A novel disulfide-linked heterodimer on pre-T cells consists of the T cell receptor beta chain and a 33 kd glycoprotein. *Cell* **75**, 283–94 (1993).

18. E. S. Hoffman, *et al.*, Productive T-cell receptor beta-chain gene rearrangement: coincident regulation of cell cycle and clonality during development in vivo. *Genes Dev* **10**, 948–62 (1996).

19. J. B. DeJarnette, *et al.*, Specific requirement for CD3epsilon in T cell development. *Proc Natl Acad Sci U S A* **95**, 14909–14. (1998).

20. M. Groettrup, A. Baron, G. Griffiths, R. Palacios, H. von Boehmer, T cell receptor (TCR) beta chain homodimers on the surface of immature but not mature alpha, gamma, delta chain deficient T cell lines. *EMBO J* **11**, 2735–2745 (1992).

21. H. von Boehmer, Unique features of the pre-T-cell receptor alpha-chain: not just a surrogate. *Nat Rev Immunol* **5**, 571–7 (2005).

22. R. M. Risueno, D. Gil, E. Fernandez, F. Sanchez-Madrid, B. Alarcon, Ligand-induced conformational change in the T-cell receptor associated with productive immune synapses. *Blood* **106**, 601–8. Epub 2005 Mar 24. (2005).

23. R. Blanco, A. Borroto, W. Schamel, P. Pereira, B. Alarcon, Conformational changes in the T cell receptor differentially determine T cell subset development in mice. *Sci Signal* **7**, ra115 (2014).

24. A. Borroto, *et al.*, Nck recruitment to the TCR required for ZAP70 activation during thymic development. *J Immunol* **190**, 1103–12 (2013).

25. A. Borroto, A. Mallabiabarrena, J. P. Albar, A. C. Martinez, B. Alarcon, Characterization of the region involved in CD3 pairwise interactions within the T cell receptor complex. *J Biol Chem* **273**, 12807–16 (1998).

26. A. Würch, J. Biro, I. Falk, H. Mossmann, K. Eichmann, Reduced generation but efficient TCR beta-chain selection of CD4+8+ double-positive thymocytes in mice with compromised CD3 complex signaling. *J Immunol* **162**, 2741–2747 (1999).

27. I. Aifantis, J. Feinberg, H. J. Fehling, J. P. Di Santo, H. von Boehmer, Early T Cell Receptor β Gene Expression Is Regulated by the Pre-T Cell Receptor–CD3 Complex. *Journal of Experimental Medicine* **190**, 141–144 (1999).

28. S. Yamasaki, T. Saito, Molecular basis for pre-TCR-mediated autonomous signaling. *Trends Immunol* **28**, 39–43 (2007).

29. A. Chao, *et al.*, Rarefaction and extrapolation with Hill numbers: a framework for sampling and estimation in species diversity studies. *Ecological Monographs* **84**, 45–67 (2014).

30. N. Martinez-Martin, *et al.*, Cooperativity between T cell receptor complexes revealed by conformational mutants of CD3epsilon. *Sci Signal* **2**, ra43 (2009).

31. X. Li, *et al.*, Pre–T cell receptors topologically sample self-ligands during thymocyte β-selection. *Science* **371**, 181–185 (2021).

32. D. Gil, W. W. Schamel, M. Montoya, F. Sanchez-Madrid, B. Alarcon, Recruitment of Nck by CD3 epsilon reveals a ligand-induced conformational change essential for T cell receptor signaling and synapse formation. *Cell* **109**, 901–12. (2002).

33. Y. Wang, *et al.*, A conserved CXXC motif in CD3epsilon is critical for T cell development and TCR signaling. *PLoS biology* **7**, e1000253 (2009).

34. J. F. Brodeur, S. Li, M. da Silva Martins, L. Larose, V. P. Dave, Critical and multiple roles for the CD3epsilon intracytoplasmic tail in double negative to double positive thymocyte differentiation. *J Immunol* **182**, 4844–53 (2009).

35. C. Xu, *et al.*, Regulation of T cell receptor activation by dynamic membrane binding of the CD3epsilon cytoplasmic tyrosine-based motif. *Cell* **135**, 702–13 (2008).

36. E. Gagnon, D. A. Schubert, S. Gordo, H. H. Chu, K. W. Wucherpfennig, Local changes in lipid environment of TCR microclusters regulate membrane binding by the CD3epsilon cytoplasmic domain. *J Exp Med* **209**, 2423–39 (2012).

37. S. Minguet, M. Swamy, B. Alarcon, I. F. Luescher, W. W. Schamel, Full activation of the T cell receptor requires both clustering and conformational changes at CD3. *Immunity.* **26**, 43-54. Epub 2006 Dec 21. (2007).

38. F. A. Hartl, *et al.*, Noncanonical binding of Lck to CD3ε promotes TCR signaling and CAR function. *Nat Immunol* **21**, 902–913 (2020).

39. M. Swamy, *et al.*, A Cholesterol-Based Allostery Model of T Cell Receptor Phosphorylation. *Immunity* **44**, 1091–1101 (2016).

40. N. Martin-Blanco, *et al.*, A window of opportunity for cooperativity in the T Cell Receptor. *Nat Commun* **9**, 2618 (2018).

41. S. Yamasaki, *et al.*, Mechanistic basis of pre-T cell receptor-mediated autonomous signaling critical for thymocyte development. *Nat Immunol* **7**, 67–75 (2006).

42. S. S. Pang, *et al.*, The structural basis for autonomous dimerization of the pre-T-cell antigen receptor. *Nature* **467**, 844–8 (2010).

43. E. Molnar, *et al.*, Cholesterol and sphingomyelin drive ligand-independent T-cell antigen receptor nanoclustering. *J Biol Chem* **287**, 42664–74 (2012).

44. F. Wang, K. Beck-Garcia, C. Zorzin, W. W. Schamel, M. M. Davis, Inhibition of T cell receptor signaling by cholesterol sulfate, a naturally occurring derivative of membrane cholesterol. *Nat Immunol* **17**, 844–50 (2016).

45. W. Yang, *et al.*, Potentiating the antitumour response of CD8(+) T cells by modulating cholesterol metabolism. *Nature* **531**, 651–5 (2016).

46. D. Bellavia, *et al.*, Combined expression of pTalpha and Notch3 in T cell leukemia identifies the requirement of preTCR for leukemogenesis. *Proc Natl Acad Sci U S A* **99**, 3788–93 (2002).

47. Y. Yashiro-Ohtani, *et al.*, Pre-TCR signaling inactivates Notch1 transcription by antagonizing E2A. *Genes Dev* **23**, 1665–76 (2009).

48. M. Tremblay, *et al.*, Modeling T-cell acute lymphoblastic leukemia induced by the SCL and LMO1 oncogenes. *Genes Dev* **24**, 1093–105 (2010).

589 49. A. Singer, S. Adoro, J.-H. Park, Lineage fate and intense debate: myths, models and
590 mechanisms of CD4- versus CD8-lineage choice. *Nat Rev Immunol* **8**, 788–801 (2008).

591 50. P. Mombaerts, *et al.*, RAG-1-deficient mice have no mature B and T lymphocytes. *Cell* **68**,
592 869–77 (1992).

593 51. K. Jaqaman, *et al.*, Robust single-particle tracking in live-cell time-lapse sequences. *Nat*
594 *Methods* **5**, 695–702 (2008).

595 52. L. Martinez-Munoz, *et al.*, Separating Actin-Dependent Chemokine Receptor
596 Nanoclustering from Dimerization Indicates a Role for Clustering in CXCR4 Signaling and
597 Function. *Molecular cell* **71**, 873 (2018).

598 53. D. A. Bolotin, *et al.*, MiXCR: software for comprehensive adaptive immunity profiling. *Nat*
599 *Methods* **12**, 380–1 (2015).

600 54. J. Shendure, H. Ji, Next-generation DNA sequencing. *Nat Biotechnol* **26**, 1135–45 (2008).

601 55. M. Shugay, *et al.*, VDJtools: Unifying Post-analysis of T Cell Receptor Repertoires. *PLoS*
602 *Comput Biol* **11**, e1004503 (2015).

603

604

## Figure Legends

**Figure 1. Reduction in size of thymic populations and impaired DN3a to DN3b transition in L19A mice.** (A) Quantification of total number of thymocytes (top panel). Each dot shows the total number of thymocytes in an individual mouse. Quantification of the number (middle panel) and percentage (lower panel) of thymocytes in the major populations defined according to expression of CD4 and CD8. Results and statistical analysis shown are based on pooled data from 67 WT and 72 L19A mice from 10 independent experiments. (B) Representative plots of the DN ($CD4^-CD8^-$) subpopulations defined by the expression of CD44 and CD25 (upper panels) and quantification in percentage (middle panel) and cell number (lower panel) of these populations in WT, L19A and *Cd3z*$^{-/-}$ mice. The DN population was pre-gated on the lineage negative ($Lin^-$) population ($CD4^-$, $CD8^-$, $CD19^-$, $B220^-$, $GR1^-$, $NK1.1^-$, $TCR\gamma\delta^-$, $CD11b^-$, $CD11c^-$, $TER119^-$). IEL precursors, identified as $Lin^-$ $CD24^{lo}CD5^{hi}TCR\beta^{hi}CD44^{lo}$ cells, were excluded from the quantifications. Graphs show the averages calculated on the basis of data obtained from 3 independent experiments with 12 WT, 12 L19A and 5 *Cd3z*$^{-/-}$ mice. (C) Representative flow cytometry plots of $Lin^-$ DN populations (defined as above) in WT, L19A and *Cd3e*$^{-/-}$ thymi according to CD44 and CD25 markers (upper panels; $CD25^{+/lo}CD44^-$ DN3 and $CD25^-CD44^-$ DN4 gates indicated) and identification of DN3a and DN3b subpopulations within the DN3 gate according to forward scatter (FSC) and CD3ζ-GFP expression (bottom panels). On the right, quantification based on pooled data from six independent experiments showing the percentage of the DN3a, DN3b and DN4 populations. (D) Representative histograms (left) and quantification (right) of the intracellular TCRβ expression levels in the DN3a ($CD44^-CD25^+$), DN3b ($CD44^-CD25^{lo}$) and DN4 ($CD44^-CD25^-$) subpopulations. Thymocytes from *Rag1*-deficient mice were used as a control for intracellular staining and were used as background control in all 3 overlays. Dashed horizontal line in graph indicates signal intensity obtained in *Rag1*$^{-/-}$ thymocytes. Quantification for one out of four experiments is shown. (E) Representative histograms (left) and quantification (right) of extracellular TCRβ expression. Data in graph represent quantification for one out of four experiments. All quantifications are presented as the mean ± SEM. P-values were calculated using unpaired two-tailed Student's t tests with 95% CI (* $p<0.05$; ** $p<0.01$; *** $p<0.001$; **** $p>0.0001$).

**Figure 2. The CD3ζ transmembrane region regulates pre-TCR-dependent signaling and function.** (A) Representative histogram of intracellular APA1/1 staining in DN3b thymocytes and box and whisker plots depicting normalized quantification of staining in DN3a, DN3b and DN4 subsets of pooled data from two independent experiments. Boxes show the median and

extend from the 25$^{th}$ to 75$^{th}$ percentile. Whiskers reach up and down to largest and smallest value, respectively, and individual data points are indicated by symbols. (B) Representative histograms and normalized quantification of intracellular pZAP70 (P-Y319) labeling. Box and whisker plots as in A. Representative histograms and quantification of expression of the CD71 (C) and CD98 (D) maturation markers at the cell surface of DN3a, DN3b and DN4 thymocytes. CD44$^-$ DN subsets were gated according CD25 levels: DN3a (CD25$^{hi}$), DN3b (CD25$^{lo}$) and DN4 (CD25$^-$). Box and whisker plots (as in A) present normalized quantification of pooled data from four independent experiments. (E) CD25 expression on DN3 (CD25$^{+/lo}$CD44$^-$) thymocytes of WT and L19A mice. Overlay of staining profiles (top) and quantification (bottom) for one out of 7 experiments quantified are shown. (F) Representative plots of BrdU staining in DN3 and DN4 populations and quantification of the percentage of BrdU$^+$ thymocytes in each population. Thymocytes shown in the plots were pre-gated on Lin$^-$CD44$^-$ population. Graphs present the mean ± sem of pooled data from three independent experiments. (G) Representative plots and quantification of Annexin V binding in indicated populations. Thymocytes shown in the plots were pre-gated on the Lin$^-$CD44$^-$ population. Quantification shows the mean ± SEM of pooled data from four independent experiments. P-values were calculated using unpaired two-tailed Student's t tests with 95% CI (* p<0.05; **p<0.01; ***p<0.001; ****p>0.0001).

**Figure 3. TIFRM analysis of the pre-TCR on CD44$^-$ DN primary thymocytes.** (A) Representative time lapse images of WT and L19A CD44$^-$ DN thymocytes. (B) Number of stable fluorescent particles detected on WT and L19A thymocytes; horizontal bars indicate mean particle number for each genotype. (C) Short time-lag diffusion coefficient ($D_{1-4}$) of the mobile particles detected in the analysis. Mean ± sem are indicated by red lines (D) Quantification of the percentage (mean ± SEM) of mobile particles for confined, free and directed diffusion tracks (E) Mean fluorescent intensity of mobile particles during the first 20 frames in which the particles are visible. Each dot in the graph presents single CD3ζ-GFP spot Mean ± SEM are indicated by red lines. Pooled data were obtained in 4 independent experiments encompassing 131 WT cells (range 20 - 57 cells/experiment) and 110 L19A cells (range 13 - 40 cells /experiment). P-values were calculated using an unpaired two-tailed Student's t test with 95% CI (***p<0.001; ****p>0.0001).

**Figure 4. TCRβ diversity of early DP and DN thymocytes in WT and L19A mice.** (A) Sorting strategy for isolation of early DP and DN3 thymocytes. (B) Number of clones per sample estimated with the richness diversity ($^0D$) for early DP thymocytes. Solid lines: Rarefaction (interpolation) curve; dashed lines: extrapolation curves; symbols: observed diversity. Note

671 that the observed values are, in all cases, close to the asymptotic part of the curves, consistent
672 with the large values of the coverage (Suppl. Fig. 3C). (C) Number of clones per sample
673 estimated for DN3 thymocytes. Meaning of lines and symbols as in B.

674

Table 1: diversity of WT and L19A TCRβ repertoires

| | WT (mean ± sd) | L19A (mean ± sd) | Statistics |
|---|---|---|---|
| *$FSC^{hi}CD69^{-}$ DP cells (#)* | *$1.4 \pm 0.8 \times 10^5$ (n=5)* | *$0.4 \pm 0.3 \times 10^5$ (n=5)* | *p=0.032 (Mann Whitney)* |
| *- In-frame Reads (#)* | *$8.4 \pm 2.0 \times 10^5$ (n=5)* | *$4.3 \pm 1.4 \times 10^5$ (n=5)* | *p=0.016 (Mann Whitney)* |
| *- Diversity Richness $D^0$* | *$7.6 \pm 4.5 \times 10^4$ (n=5)* | *$2.3 \pm 1.5 \times 10^4$ (n=5)* | *p=0.032 (Mann Whitney)* |
| *- Estimated Richness* | *$7.9 \pm 4.7 \times 10^4$ (n=5)* | *$2.4 \pm 1.5 \times 10^4$ (n=5)* | *p=0.032 (Mann Whitney)* |
| *$CD25^{hi}CD44^{-}$ DN cells (#)* | *$8.6 \pm 5.2 \times 10^4$ (n=4)* | *$8.2 \pm 1.9 \times 10^4$ (n=2)* | *p=0.800 (Mann Whitney)* |
| *- In-frame Reads (#)* | *$1.3 \pm 1.4 \times 10^5$ (n=4)* | *$3.6 \pm 0.3 \times 10^5$ (n=2)* | *p=0.133 (Mann Whitney)* |
| *- Diversity Richness $D^0$* | *$1.1 \pm 0.9 \times 10^4$ (n=4)* | *$1.4 \pm 0.5 \times 10^4$ (n=2)* | *p=0.530 (Mann Whitney)* |
| *- Estimated Richness* | *$1.2 \pm 0.9 \times 10^4$ (n=4)* | *$1.4 \pm 0.5 \times 10^4$ (n=2)* | *p=0.533 (Mann Whitney)* |

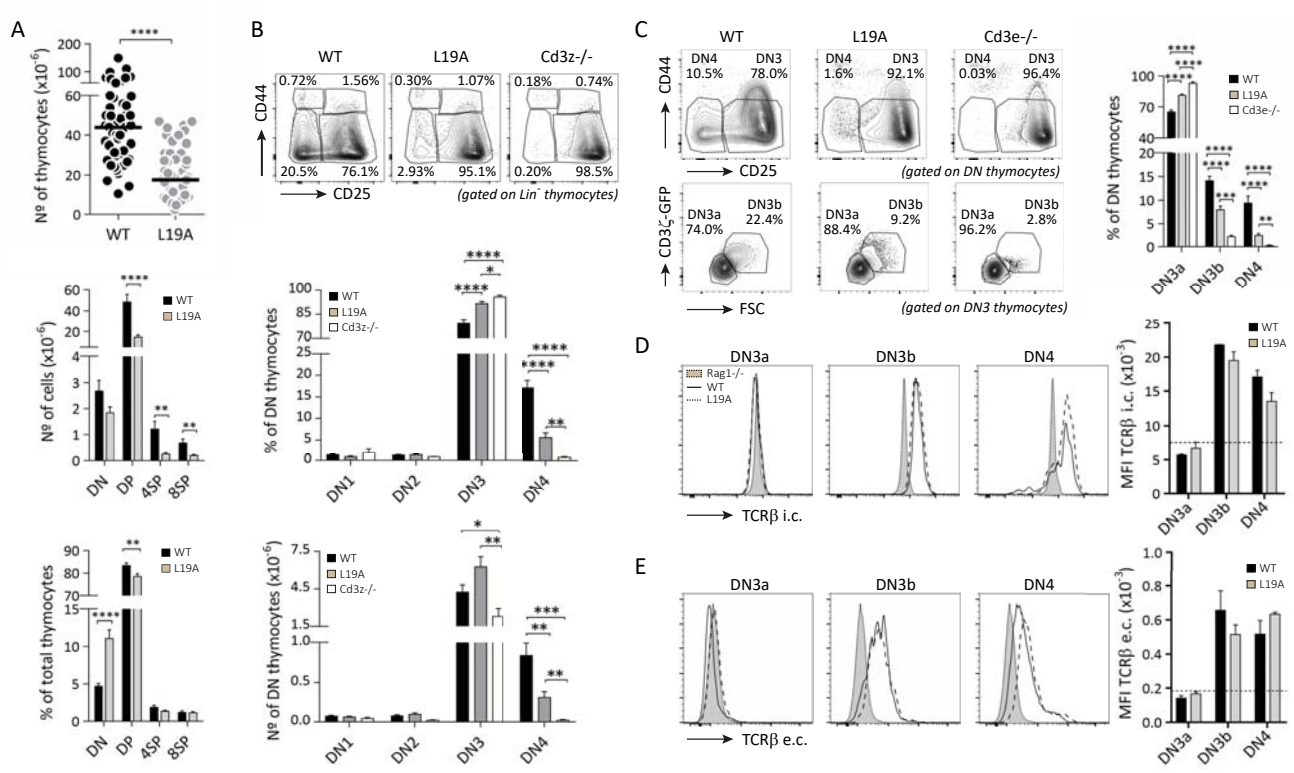


*Bovolenta et al., Figure 1*

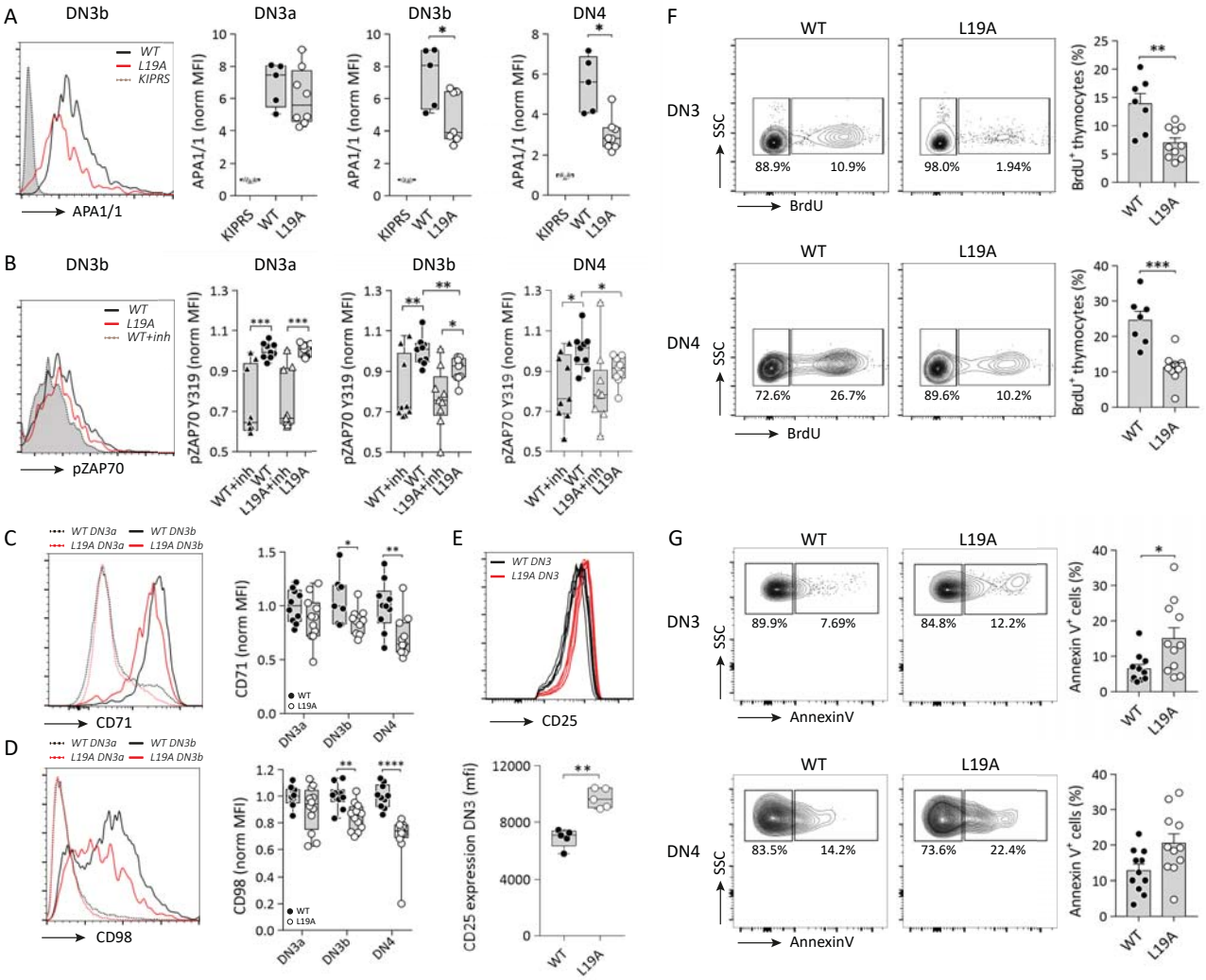


*Bovolenta et al., Figure 2*

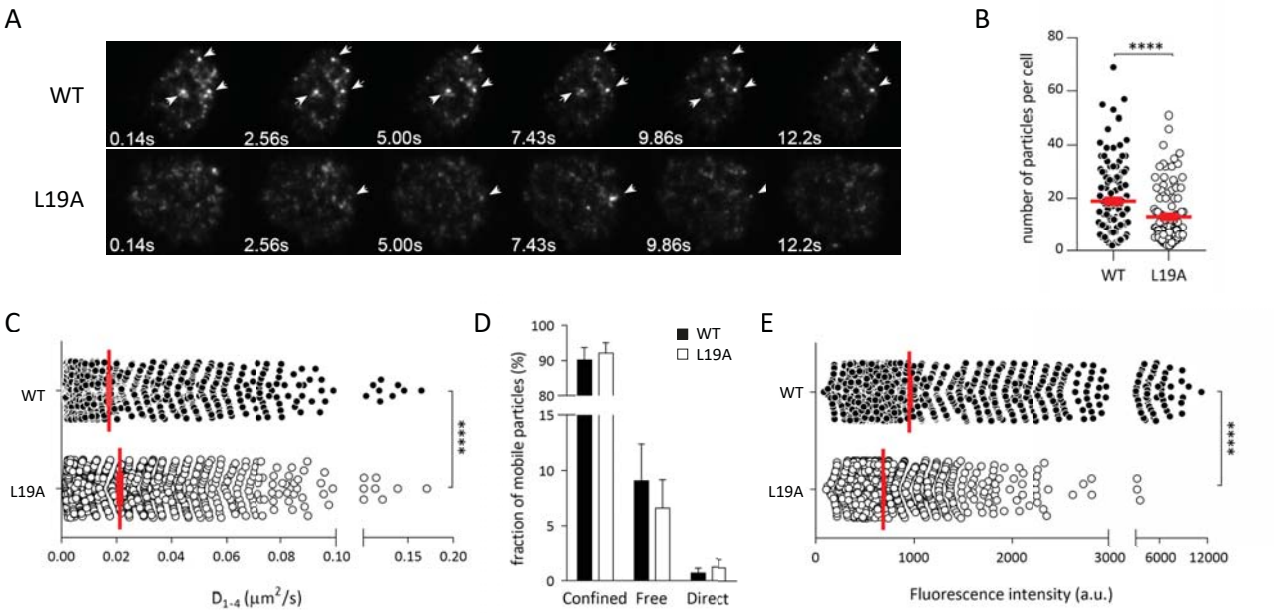


*Bovolenta et al., Figure 3*

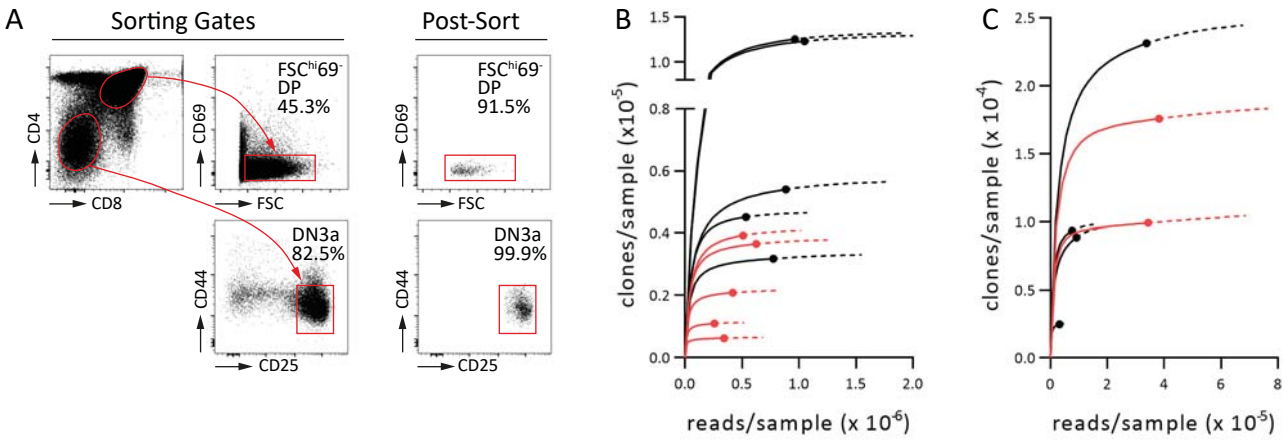


*Bovolenta et al., Figure 4*